Transient simulation of magnetic bearing and backup bearing interaction in a high speed rotary atomizer subjected to impulsive loads

Lawrence HAWKINS*, Zhiyang WANG* and Vishal Wadhvani**

*Calnetix Technologies

16323 Shoemaker Avenue, Cerritos, CA 90703 USA

E-mail: lhawkins@calnetix.com

**Dedert Corporation

Homewood, IL USA

Abstract

A high speed rotary atomizer supported by active magnetic bearings (AMB) has been in service in a pharmaceutical-processing plant for over three years. This process challenges the AMBs by imposing variable, quasi-periodic external impulses on the atomizer. The impulses are occasionally large enough to overload the AMBs, resulting in backup bearing contact during operation. Implementation of a novel impulse detection and Impulse Recovery Compensator (IRC) introduced to allow continuous operation has been previously reported. In this work, a transient, nonlinear rotordynamic simulation of the atomizer, together with field measured position and current time histories, is used to help characterize the impulsive loads, the magnetic bearing control response and backup bearing reaction loads. The simulation results provide a reasonable match to field measured position and current time histories when the impulse load is produced by a sudden large unbalance, temporary or permanent. The simulation correctly predicts that amplifier saturation is relieved and the rotor re-levitates when the control is switched to the IRC. Predicted backup bearing loads during whirl are reasonable and subsequently calculated stress levels are consistent with favorable inspections of backup bearings removed from service. Future work with the simulation will include further improvements to the amplifier and backup bearing modelling.

Keywords : Active Magnetic Bearing, Magnetic Bearing Control Design, Touchdown Bearings, Backup Bearings, Rotary Atomizer.

1. Introduction

Rotary disc atomizers are an integral part of the spray drying process employed in many pharmaceutical and food processing applications. In a rotary atomizer, slurry is fed into a hollow wheel spinning at high speed. Contact with the wheel accelerates the slurry up to the wheel peripheral speed as it exits through nozzles in the wheel periphery. As the slurry exits the wheel into a large chamber, it breaks into near equal size droplets. Hot air blown into the chamber around the wheel quickly dries the slurry droplets into fine particles, typically on the order of 100 to 200 µm (0.0039 to 0.0079 inch). The size of the dried particles (the end product) is inversely proportional to nozzle tip speed along with a number of other parameters. Figure 1 is a cutaway rendering of the atomizer installed in a spray dryer.

Conventional rotary atomizers have been used for many years, typically with the atomizer wheel drive shaft supported by rolling element bearings and driven by a conventional motor through either a speed increasing gearbox or drive belt. These atomizers have several limitations including limited atomizer wheel surface speed, limited speed adjustment range, short bearing life, and maintenance intensive lubrication systems. To address the limitations with existing designs, a direct drive atomizer with a high-speed, synchronous motor supported on AMBs was developed and has been in service in a pharmaceutical-processing plant for over three years. This approach enables surface speeds up to 274 m/s (900 fps) at the 16,000 rpm maximum speed, 50% higher than was possible with the previous design. This

Magnetic Spray Machines (MSM-250) is more efficient and has higher power density than the conventional machine it replaced allowing substantial increases in product feed rate and hence dryer production.

The first field installation of the MSM-250 was in a spray dryer used for the production of pharmaceutical dry powders. This application required a nominal operating speed range of 12,000-13,000 rpm. Soon after field operation commenced, it became clear that in addition to the expected moderate variations in synchronous load the atomizer was subject to frequent non-periodic impulse loads. The continuously changing synchronous load was easily accommodated by the AMB control system and standard synchronous cancellation algorithm. The frequently observed impulse forces vary significantly in magnitude with low level impulses occurring several times a second, whereas impulses large enough to cause backup bearing contact are much less frequent. When the units were initially field commissioned in August 2012, the atomizers were experiencing impulses large enough to cause backup bearing contact several times per hour. More concerning, impulses large enough to prevent recovery of the rotor to stable operation (causing a vibration trip) occurred several times per month and occasionally several times per week.

As the atomizer could run continuously at full power when supplied with water instead of slurry, efforts to mitigate or eliminate the effect of the impulse loading focused on the characteristics of the slurry. While the majority of applications for the MSM-250 will use slurry with a dynamic viscosity less than 1 Pa-s, this particular application uses slurries with a dynamic viscosity greater than 30 Pa-s. Further, these products are highly thixotropic (viscosity varies with shear history) and have a strong tendency to form lumps in slurry form. They also have a tendency to form an uneven build up on the bottom surfaces of the atomizer wheel, later breaking off irregular pieces (Fig. 2). Any or all of these slurry characteristics were suspected as the source of the unusual rate of impulse loading.

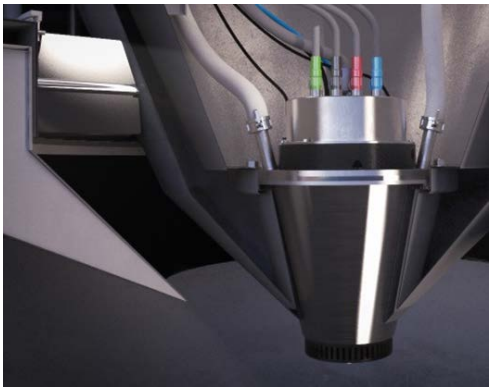

Fig. 1. Atomizer installed in Spray Dryer.

Fig. 2. Atomizer wheel with uneven buildup.

A number of design and software changes were implemented to allow the atomizer to overcome the challenges posed by this installation and to reach sustained, continuous operation. Some of the changes were reported in-depth by Khatri, et al. (2015) – the changes are summarized and updated here:

1) Auto Relevitation. Calnetix normal response to sustained contact with the backup bearing is to de-levitate the rotor and request a trip to spin down the machine. Since the overloading impulse forces appeared to be transient, an auto-relevitation feature was introduced to reduce the number of trips. When enabled, this feature optionally suppresses the trip request, waits an adjustable time delay, and then attempts to re-levitate the rotor.
2) Increase Magnetic Bearing Stiffness. An obvious step to reduce the number of contacts events was to increase the magnetic bearing compensator gain (stiffness), reducing shaft motion for a given impulse load.
3) Process Improvements. The slurry processing and feed system was examined for possible mechanisms for the impulse forces. Several candidates were identified: a) large dense materials passing through to the atomizer, either from lumps in the slurry or foreign material, b) product flow through the long feed pipe causing occasional surges up or down in the flow rate, and c) product sticking on the bottom of the spinning disc in irregular patterns. To address item a), a strainer was installed on the feed line immediately preceding the atomizer. This resulted in a significant reduction in the number of contact events that resulted in delevitation. To address item b) a high shear pump was installed next to the strainer. This offered some limited benefit at the time and was removed, but is available for future trials. To address item c), four different food grade

coatings were used on the atomizer wheels and one was selected based on a reduced incidence of intermittent backup bearing contacts.

4) Impulse Recovery Feature. Increasing the magnetic bearing stiffness reduced the number of backup bearing contact events, but the rate of failed relevitation events unexpectedly increased. This was determined to be due to the either (or both): a) saturation of the amplifiers due to the now higher slew rate needs from the stiffer compensator when the rotor is displaced to the backup bearings, or b) due to phase lag (negative damping) at the frequency of the rotor rigid body modes when in contact with the backup bearings. To address this, an impulse recovery feature was created for the MBC. This feature switches control automatically to a different compensator, referred to as The Impulse Recovery Compensator (IRC), once backup bearing contact is detected. The compensator used at backup bearing contact (IRC) is much softer than the primary compensator and thus doesn't result in a current command that will exceed the slew rate with synchronous whirl at backup bearing clearance. The IRC also has positive phase margin out to 400 Hz, well beyond the expected rigid body mode frequencies and the maximum synchronous frequency.

Both the increase in magnetic bearing stiffness and the process improvements reduced but did not eliminate the incidence of impulse loading and subsequent intermittent contact (IC) with the backup bearings. The auto relevitation feature resulted in near continuous operation of the atomizer, but there were still occasional failed re-levitations (25% unsuccessful). Introduction of the IRC reduced the number of failed auto relevitation events; however, over the ensuing year of operation, up to one failed relevitation per month was observed. When the IRC was first introduced, a 180 second lock out period was included to prevent potential continuous triggering of the IRC. Examination of field data has shown that every failed relevitation (from an impulse overload event) happened during a time window when the IRC was locked out of operation. Changes to ensure the IRC was always available on a relevitation attempt have eliminated failed re-levitations – no occurrences and no trips over the nine month period since implementation. Additional changes to allow multiple triggers within a shorter lock out time have eliminated de-levitations – no occurrences over the four month period since implementation.

Although sustained, continuous operation has been achieved, the atomizer still sees enough overload impulse events to produce 10-12 intermittent contact (IC) events per day. These events are being monitored and the number allowed for a given backup bearing set has been steadily extended based on visual inspections of the backup bearings. The most recent set of backup bearings are allowed 1500 IC events and are expected to be removed after ~4.5 months, putting the targeted 6 month replacement cycle in sight. The backup bearings are replaced on-site within a few hours, and the replacement can be scheduled around planned plant shutdowns.

Notwithstanding this progress, there has been a poor understanding of the magnitude and nature of impulse loading as well as the loads sustained by the backup bearings. Better insight into these issues will improve future designs and assist in the assessment of backup bearing life. To this end, a transient, nonlinear rotordynamic simulation of the atomizer was used together with field measured position and current time histories to help characterize both the impulsive loads imposed on the rotor and the magnetic bearing and backup bearing loads reaction loads. The field measurements are discussed next, covering two scenarios of interest. Following that is a description of the simulation model and simulation results.

2. Field measurements

Two sets of field measurements that will be the target of simulations are discussed here. Figures 3-6 show an example of a hard contact event that resulted in a delevitation and recovery while spinning at the standard operating speed of 12,500 rpm. In this set of data the IRC was locked out and so was not used at contact. Figure 3 shows a 3 second time slice from one of the upper position sensors. The impulse occurs at 151 seconds into this data set, resulting in radial backup bearing contact and a full forward whirl at 175-180 Hz. Since levitation was not recovered on initial contact, the rotor was delevitated at just past 151.6 sec (the fault detection scheme has a 0.6 sec delay). The rotor is then relevitated by the Auto Relevitation feature after an additional 0.5 second delay. The 0.5 second delay is used in case the impulse was caused by a clump of product in the wheel that needed time to exit.

Figure 4 shows a plot of the radial displacements from both the lower and upper magnetic bearing sensor pairs (Brg 1 Position, Brg 2 Position respectively) and the axial bearing. As is typical for these events, the fault limit is first

exceeded at the lower bearing and then followed by the upper bearing. In this case, the lower magnetic bearing regains levitation, whereas the upper magnetic bearing cannot regain levitation. Also, typical for these events, the axial bearing maintains levitation throughout. Figure 5 shows that there is a full forward whirl at the upper bearing.

Figure 6 shows time history of the radial position, current command and coil current from the x2 axis of the upper bearing. The coil current should follow the command with a very small phase lag at these frequencies, but two to three cycles after contact, the slew rate limit of the amplifier is reached and the coil current lags the command. The result is additional and unintended phase lag that results in the magnetic bearing driving the forward whirl instead of abating it.

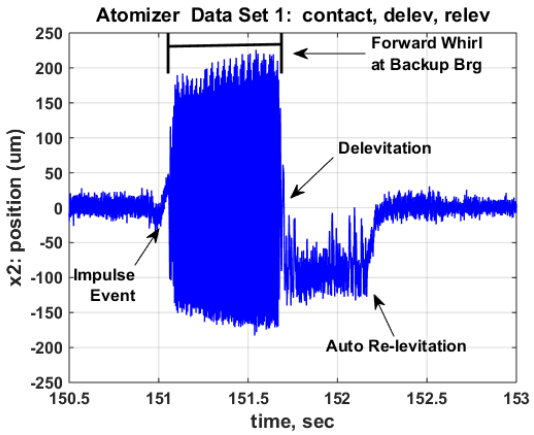

Fig. 3. Radial position vs. time during an impulse overload, backup bearing whirl, delev and relev event.

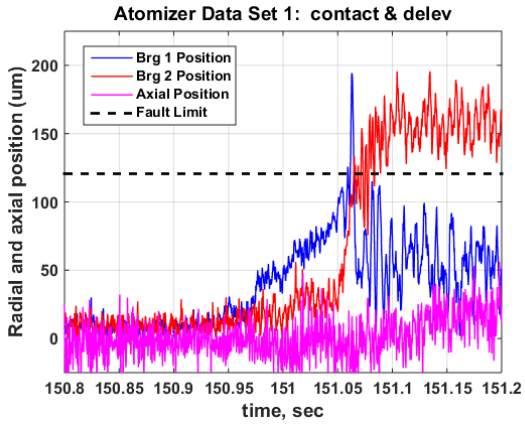

Fig. 4. Radial and axial positions vs. time during impulse overload and backup bearing contact.

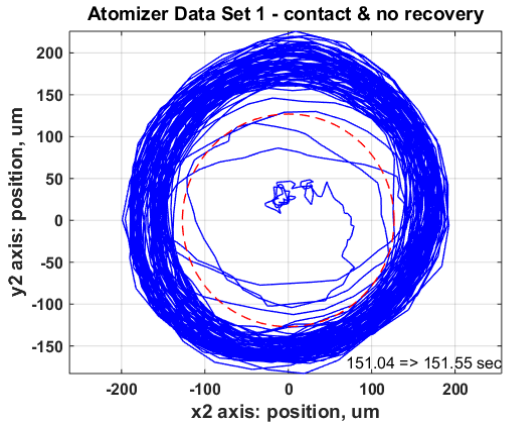

Fig. 5. Orbit at upper radial position sensors during impulse and backup bearing whirl (151.04-151.55 sec).

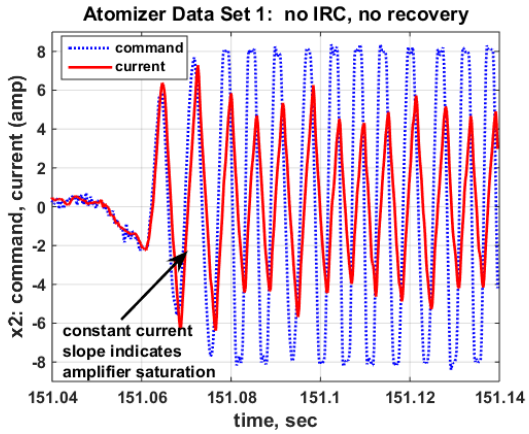

Fig. 6. Current command and coil current vs. time during backup bearing whirl, showing saturation.

As previously mentioned, a stiff primary magnetic bearing compensator is used to limit the number of backup bearing contacts that would otherwise result from the numerous low level impulse loads. This has the downside of making it much easier to saturate the amplifier in the event of a hard contact. This was the reason for the development of the IRC feature. At the time the data in Figs. 3-6 was collected, the system was set up such that the IRC was always used for a relevitation event; however, it still had a 5 second timeout period between triggers. The IRC feature was locked out in this example because there had been previous contact only a few seconds before.

Figures 7-8 show a second field measured example, this one for a hard contact, but with no loss of levitation. Figure 7 is an orbit plot of *x* vs. *y* axis data from the upper magnetic bearing position sensors. The rotor goes into full whirl around the backup bearing for a few cycles and then recovers. Figure 8 shows time history of the current command and coil current from one axis of the upper bearing. As with the previous example, the amplifier is saturated after the first few cycles. However, in this case the control is switched to the IRC compensator at 158.25 seconds (0.05 sec after the fault limit is reached). The lower gain of the IRC results in a smaller current request at the whirl frequency. This allows the saturation to quickly clear and the magnetic bearings to recover levitation.

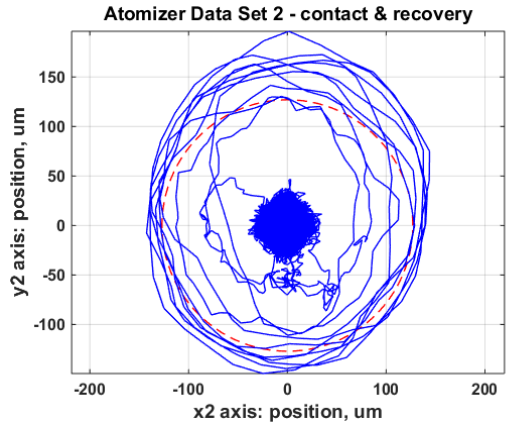

Fig. 7. Orbit at upper radial position sensors during impulse and recovery.

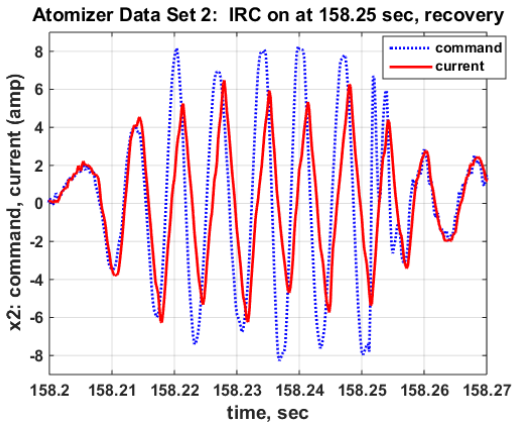

Fig. 8. Current command and coil current vs. time; IRC activates at 158.25 sec.

3. Transient, non-linear simulation

A transient, nonlinear rotordynamic simulation of the atomizer was developed to help characterize the impulsive loads, the magnetic bearing control response and backup bearing reaction loads. In this analysis, the rotordynamic equations of motion for a coupled rotor/housing system represented in second order form are:

$$\begin{bmatrix}\mathbf{M}_R & 0\\ 0 & \mathbf{M}_C\end{bmatrix}\begin{Bmatrix}\ddot{\mathbf{q}}_R\\ \ddot{\mathbf{q}}_C\end{Bmatrix}+\begin{bmatrix}\mathbf{D}_R+\mathbf{G}_R & 0\\ 0 & \mathbf{D}_C\end{bmatrix}\begin{Bmatrix}\dot{\mathbf{q}}_R\\ \dot{\mathbf{q}}_C\end{Bmatrix}+\begin{bmatrix}\mathbf{K}_R & 0\\ 0 & \mathbf{K}_C\end{bmatrix}\begin{Bmatrix}\mathbf{q}_R\\ \mathbf{q}_C\end{Bmatrix}+\begin{bmatrix}\mathbf{K}_{act11} & \mathbf{K}_{act12}\\ \mathbf{K}_{act21} & \mathbf{K}_{act22}\end{bmatrix}\begin{Bmatrix}\mathbf{q}_R\\ \mathbf{q}_C\end{Bmatrix}=\begin{Bmatrix}\mathbf{f}_{mb,R}\\ \mathbf{f}_{mb,C}\end{Bmatrix}+\begin{Bmatrix}\mathbf{f}_{ext,R}\\ \mathbf{f}_{ext,C}\end{Bmatrix} \quad (1)$$

where the subscripts R and C refer to rotor and housing structures, **M**, **D** and **K** are the mass, damping and stiffness matrices, for the separate rotor and housing structures, $\mathbf{G}_R$ contains skew symmetric products of polar inertia and spin speed, $\mathbf{K}_{act}$ is a sparse matrix containing the passive actuator negative stiffness, and **q** is the physical displacement vector. Magnetic bearing control forces are applied through the force vector, $\mathbf{f}_{mb}$. The external force vector $\mathbf{f}_{ext}$ can include linear, nonlinear and/or time dependent forces such as rotor unbalance forces, point static or impulse loads or external vibration inputs. The simulation tool is a further enhancement of the tool described by Hawkins, et al (2006).

The equations of motion are integrated with a Newmark-β algorithm using a time step varied from 1 to 10 µsec. The magnetic bearing control is updated at the same rate used in the MBC hardware: a) the current command is updated every 80 µsec, and b) the coil currents are updated from the command every 40 µsec.

Initial simulations used a maximum *di/dt* calculated from (Vischer, 1990):

$$di/dt)_{max} = (V_{bus} - R\,i - K_i v)/L \quad (2)$$

where V_{bus} is the overhead voltage, R is coil resistance, i is coil current, K_i is force/current factor, v is max whirl velocity, and L is coil inductance. However, the maximum currents slew rate from Fig. 6 was about 15% lower than the calculation of Eq. (2) so the measured value was used. The difference could be because it is only correct to use K_i in Eq. (2) in the ideal case (Schweitzer and Maslen, 2009). In future work, this assumption will be examined and the maximum slew rate will be calculated from Eq. (2) on a transient basis as part of the simulation. Modelling the current control loop directly will also be considered.

3.1 Elements of the system model

The elements of the system model are shown in Fig. 9. This model includes:

1) Rotor. A linear, flexible structural dynamic rotor model.
2) Housing. A linear, rigid housing model that matches the mass distribution of the housing.
3) Backup bearing. The backup bearing stiffness is modelled with a nonlinear force/deflection curve to represent the ball/race compliance along with an experience based damping coefficient. The ball/race contact stiffness and

the rotor/backup bearing contact stiffness are quite high relative to the resilient mount stiffness (below). The free radial clearance between the backup bearing inner ring and the rotor is 127 µm (0.005 inch) per nominal design clearance. The axial/radial coupling proposed by Wilkes, et al. (2013) is included in the simulation tool, but doesn't affect the results as the axial bearing remains levitated during the atomizer contact events.

4) Resilient mount. The resilient mount model includes the mass of the mount and backup bearing outer rings, linear stiffness and damping coefficients representing the O-ring supports, and a hard stop in parallel with the O-rings that allows 77 µm (0.003 inch) radial travel before engaging.

5) Magnetic bearing. The magnetic bearing compensator is represented by the same discrete coefficients used in the Magnetic Bearing Controller (MBC). Sensor, amplifier and time delay dynamics are included and based on measured values. Nonlinearities include actuator force saturation, amplifier slew rate limit, and integrator windup limit. The magnetic bearing actuators used in this machine have a permanent magnet bias so the passive radial negative stiffness remains in the model at the electromagnet locations even if the bearings are deactivated.

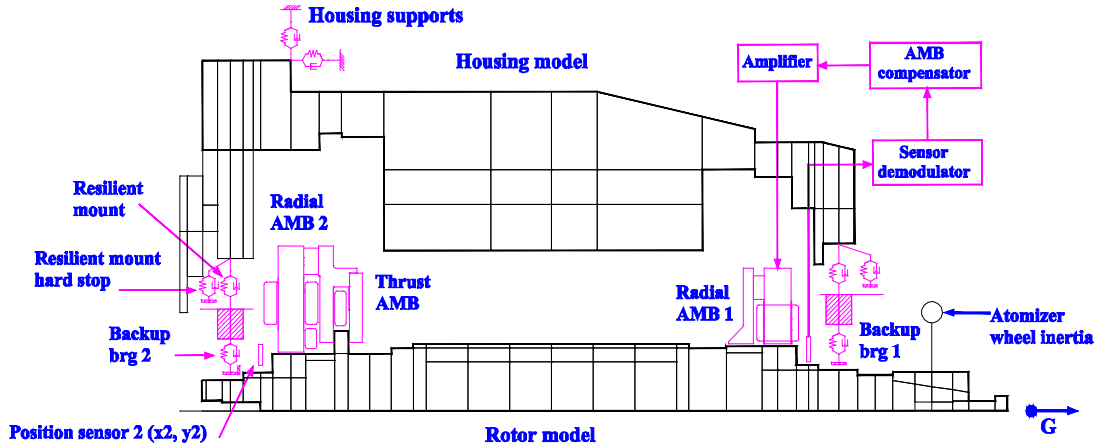

Fig. 9. System model includes rotor, housing, AMB, and backup bearing. Atomizer model is shown rotated 90 degrees counter clockwise.

4. Simulation results

A series of simulations were run to define load characteristics that would produce predicted responses similar to field observations (Figs. 3-8). Several different types of radial loads were applied at the atomizer wheel: a) suddenly applied and maintained static load, b) suddenly applied static load of 0.3 second duration, c) suddenly applied and maintained unbalance, d) suddenly applied unbalance of 0.3 second duration. Several different magnitudes of each load type were applied. Static loads of sufficient amplitude resulted in backup bearing contact but not whirl whether temporary or permanent. Sudden unbalance loads whether temporary or permanent, sufficient to cause hard contact consistently produced whirl at both backup bearings. The minimum unbalance that would saturate the amplifiers and a produce sustained whirl was 70 gm-in. This is equivalent to about 16 cm^3 (1 in^3) of dried product breaking off near the wheel rim or a larger amount breaking off at a smaller radius.

Figures 10-11 show the results of a simulation (Case 1) where a timed unbalance of 70 gm-in is applied at the wheel at 0.05 seconds and removed at 0.08 seconds. The nominal magnetic bearing compensator is used without switching to the IRC. This simulation was intended to match the measurements in Figs. 5 and 6. Figure 10 shows predicted displacement orbit at the Brg2 position sensors. The rotor contacts the backup bearing and the orbit increases until equilibrium is reached at 0.011 inch. Figure 11 shows time history of the radial position, radial current command and radial coil current from the x2 axis of the upper bearing.

The predicted whirl frequency of about 170 Hz for the simulation is a good match to the measured value of 175-180 Hz. As with the field measurements, the rotor remains in whirl even after the unbalance is removed – driven by the phase lag produced by saturation. The predicted characteristics are a generally good match to the test data except that the predicted orbit radius at the position sensor is about 35% higher than the measured value. Also, the simulation routinely predict whirl at both the upper and lower backup bearings, whereas in 60% of the field measurements, sustained whirl only occurs at the upper backup bearing. Some of the reasons for this discrepancy could include: 1)

nominal values, particularly clearances and travel limits, are used in the simulation and the actual machine values may be different, 2) the model does not currently include moment stiffness for the backup bearings, and 3) the maximum slew rate in the real machine will vary with rotor velocity and this is not accounted for the in the model.

Figures 12-13 show the results of a simulation (Case 2) identical to the previous case except that the control switches from the nominal compensator to the IRC at 50 msec after impending backup bearing contact is detected. This simulation was intended to match the measurements in Figs. 7 and 8. Figure 12 shows predicted displacement orbit at the Brg2 position sensors. The rotor stays in contact with the backup bearing for about 8 cycles, with the highest excursion reaching 250 µm (0.010 in). By comparison, the highest excursion in the measurement of Fig. 7 was 203 µm (0.008 in). Figure 13 shows time history of the current command and coil current from the x2 axis of the upper bearing. The simulation again correctly predicts the general character of the event. Once the IRC is activated, the simulation shows recovery in a similar fashion to the measurement.

Figure 14 shows predicted loads for the upper backup bearings for the two simulation cases. For Case 1 where the rotor stayed in full whirl around the backup bearings, the load levels out to about 10,000 N (2,240 lbf) for the duplex pair at the maximum whirl radius. The maximum Hertzian contact stress for this load is in the range of 2800-2900 MPa. This is an acceptable level for short duration events such as the 0.6 sec time delay for the MBC fault to trigger. Once the fault sequence times out and the rotor is delevitated, the load drops to less than 2,230 N (500 lbf) per bearing set. Further, inspections of bearings removed from the machine after as many as 30 delevitation events do not exhibit signs of severe stress or Brinelling. It also should be noted that this type of event has been essentially eliminated by use of the IRC. For Case 2 where the transition to the IRC allows levitation to recover within a few cycles, the peak load reached was 8,800 N (1,975 lbf). The peak stress for this case is about 100 MPa less than Case 1 and only occurs on 2 cycles compared to 100 cycles for Case 1.

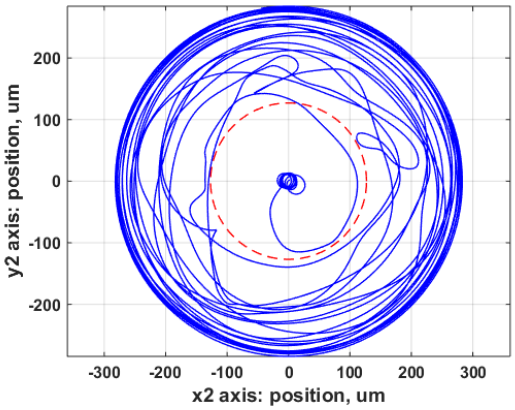

Fig. 10. Simulation 1 position orbit; impulse from sudden unbalance followed by backup bearing whirl w/no IRC.

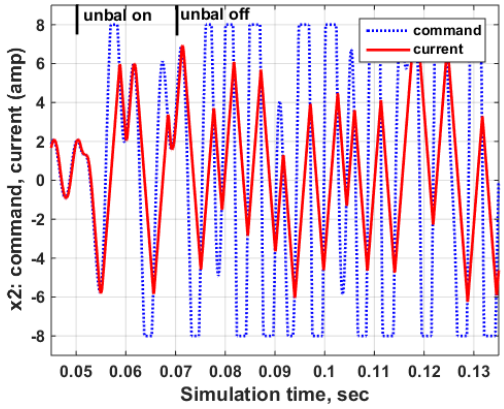

Fig. 11. Simulation 1: command and coil current vs. time; during impulse, whirl, & amplifier saturation.

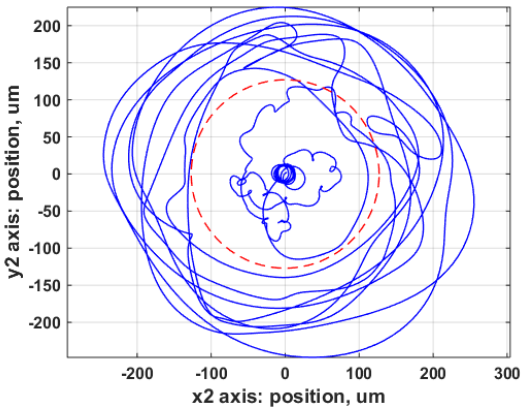

Fig. 12. Simulation 2 position orbit; impulse from sudden unbalance, backup bearing contact and recovery; w/IRC

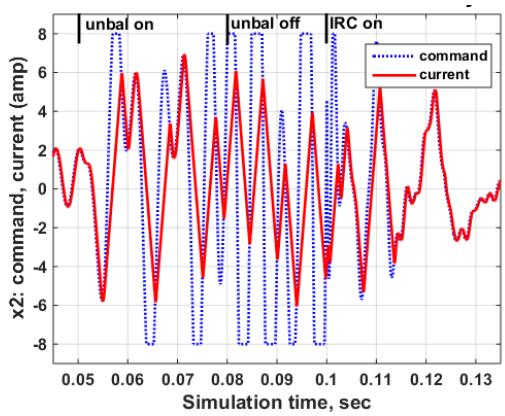

Fig. 13. Simulation 2: command and coil current vs. time; during impulse, amplifier saturation and recovery.

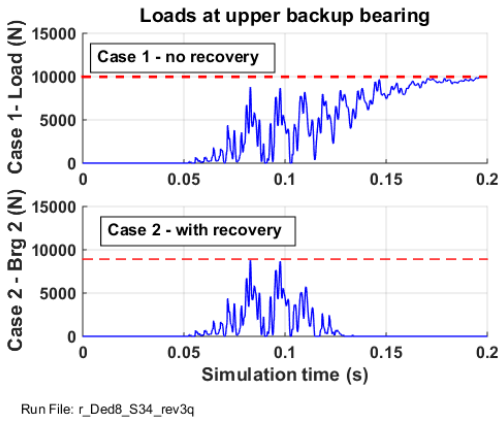

Fig. 14. Predicted radial loads at the upper backup bearing for the two simulation cases.

5. Conclusions

A high speed rotary atomizer supported by magnetic bearings is subjected to variable process impulse loads that cause backup bearing contact several times per day. A transient, nonlinear rotordynamic simulation was used to study the impulse events to assess nature of the impulse loads, to characterize the backup bearing loads, and to confirm the action of the IRC in allowing recovery from whirl in the backup bearing. The simulation showed:

1) Overall, the simulation produces a reasonable match to field measured position, current command, and coil current time histories. However, the amplitudes of the sensed relative rotor housing positions were high relative to measured values. This is likely due to either: a) the backup bearing model which does not include any moment stiffness, or b) due to imprecise knowledge of actual resilient mount stiffness and clearance.
2) Whirl at the backup bearings is predicted by the simulation when the impulse load is due to a large change in unbalance (either temporary) of permanent. This is likely due to lumps of dense product passing through the wheel but may also be caused by sudden loss of dried product from the exterior wheel surfaces.
3) The simulation does not predict whirl if the impulse load is a radial pulse or short or long duration radial load.
4) Whirl at the backup bearings is predicted by the simulation when the amplifiers are driven to saturation by the high dynamic current requirement imposed by the combination of high whirl frequency, high amplitude, and the high stiffness needed to avoid impulses. When the unbalance load is removed, the whirl sustains driven by the phase lag caused by the saturation. This behavior matches field data.
5) The simulation always predicts whirl at both backup bearings whereas only 40% of the field data show this.
6) The simulation predicts levitation recovery by switching to the IRC in the same manner observed in field data. The lower gain and positive phase lead at the whirl frequency of the IRC produces a stabilizing control force.
7) The backup bearing loads during whirl are sustainable for the atomizer backup bearing, particularly for the short duration required to trigger a fault or other action.

References

Khatri, R., Hawkins, L., Bazergui, C., Demonstrated operability and reliability improvements for a prototype high-speed rotary-disc atomizer supported on active magnetic bearings, ASME Turbo Expo, GT2015-43803 (2015).

Wilkes, J., Moore, J., Ransom, D., Vannini, G., An improved catcher bearing model and an explanation of the forward whirl/whip phenomenon observed in active magnetic bearing transient drop experiments, ASME Turbo Expo, GT2013-94594 (2013).

Hawkins, L.A., Imani, S., Filatov, A., Prosser, D., Test results and analytical predictions for rotor drop testing of an expander/generator, ASME Turbo Expo, GT2006-90283, (2006).

Schweitzer, G., Maslen, E.H, Magnetic bearings: Theory, design, and application to rotating machinery, Springer Verlag, Berlin, p.48.

Vischer, D., Bleuler, H., A new approach to sensorless and voltage controlled AMBs based on network theory concepts, Proceedings 2nd International Symposium on Magnetic Bearings, (1990).